An Experimental Investigation of Unsteady Pressure Distribution on Tandem Heliostats

Azadeh Jafari,[1, a)] Matthew Emes,[1, b)] Benjamin Cazzolato,[1, c)] Farzin Ghanadi,[2, d)] Maziar Arjomandi[1, e)]

[1] *Centre for Energy Technology, School of Mechanical Engineering, University of Adelaide, Adelaide, SA 5005, Australia*
[2] *School of Engineering, University of Newcastle, Callaghan, NSW 2308, Australia.*

[a)] Corresponding author: azadeh.jafari@adelaide.edu.au
[b)] matthew.emes@adelaide.edu.au
[c)] benjamin.cazzolato@adelaide.edu.au
[d)] farzin.ghanadi@newcastle.edu.au
[e)] maziar.arjomandi@adelaide.edu.au

Abstract. The unsteady surface pressure distribution on heliostats in a tandem arrangement is investigated in this experimental study. The differential pressure on the panel of a heliostat model is measured for a range of gaps between the two tandem heliostats, varying from 1 to 7 times the chord length dimension of the panel. The heliostat models are placed in a simulated turbulent atmospheric boundary layer in the University of Adelaide wind tunnel. The measured surface pressures are analysed and compared with those of a single heliostat, at three elevation angles of 30°, 60° and 90°. The results showed that the peak pressure distribution on the tandem heliostat differs significantly from the single heliostat. Regions of large-magnitude pressure occur near the edges of the panel at smaller gap ratios. Large unsteady variations of the position of the centre of pressure are found for the tandem heliostat at gap ratios equal to and less than 5, which lead to an increase of the hinge moment relative to the single heliostat. The peak hinge moment coefficient on a tandem heliostat is found to be 40% and 70% larger than the coefficient on the single heliostat at elevation angles of 30° and 60°, respectively. The results therefore indicate the importance of the unsteady wind loads in different rows of a field for the design of heliostats as they vary significantly from the loads on a single heliostat dependent on the field arrangement.

INTRODUCTION

The turbulence within the atmospheric boundary layer induces unsteady aerodynamic loads on heliostats. Mean and peak wind loads on isolated heliostat models at different operating conditions have been studied by wind tunnel experiements [1-4]. Wind loads in a heliostat field are however different from an isolated heliostat. Heliostats act as bluff bodies within the flow and due to the interference of their wakes with each other, the aerodynamics of multiple bluff bodies differ from a single bluff body and depend on the arrangement of the bodies and the spacing between them. The vortices shed by an upstream body can impose vibrations and fluctuating loads on the downstream structures, especially if situated in their intermediate wake areas. Hence, the arrangement of heliostats in a field and the spacing between them is an important parameter that affects the wind loads on heliostats in different rows of the field. The gap between subsequent rows of a heliostat field typically varies from a value equal to the chord length of the mirror panel to about 8-times the chord length as the heliostats are installed further away from the central tower [5]. Wind tunnel experiments on heliostats in an array arrangement show that decreasing the spacing between heliostats reduces loads on the heliostats in inner rows due to the blockage effect of upstream heliostats [6]. Peterka *et al.* [7] measured the drag and hinge moment coefficients on a heliostat in the fourth row of a four-row arrangement with low and high densities. They reported that the mean drag force and hinge moment coefficients are about 10% to 50% less than the loads on a heliostat in the first row [7]. In contrast, the peak drag force on the heliostat in the fourth

row was found to be 40% larger than that on a heliostat in the first row [7]. Emes et al. [8] reported that for two sequential heliostats in stow position the peak lift force on the second tandem heliostat is 47% less than the isolated stowed heliostat. Yu et al. [9] found that the peak drag coefficient on an operating heliostat in tandem configuration is up to 50% less than the isolated heliostat when the gap betwen the two heliostat pylons is between 2 to 3 times the chord length dimension of the mirror panel.

More important than the lift and drag forces is the distribution of pressure loads on the mirror panel, which is decisive for the design of the heliostat structure. The unsteady pressure distributions on the mirror panel impose unsteady moments at the heliostat hinge and base, which can lead to critical load conditions for the heliostat drives, pedestal and foundation. It is therefore necessary to gain an understanding of the variations of the unsteady moments for the design of heliostats. Moreover, the pressure distributions on in-field heliostats are influenced by the wake and shielding effect of the upstream operating heliostats. However, the unsteady pressure distributions on heliostats in a field have not been studied in the literature. Hence, in this study, the pressure distribution on a heliostat in tandem arrangement at different operating conditions is investigated, and the effect of the gap spacing between the two tandem heliostats is studied. The surface pressure distributions are analysed and compared to the single heliostat. Furthermore, the effect of the unsteady pressure distributions on the hinge moment of the tandem heliostat is investigated. The variations of the hinge moment are crucial for determination of the critical load conditions of the elevation drive, and hence provide an insight into design of heliostats for a field arrangement.

METHODOLOGY

Experiments were conducted in a large-scale wind tunnel at the University of Adelaide. The test section of the boundary layer wind tunnel has a cross-sectional area of 3 m × 3 m and a development length of 17 m. Atmospheric boundary layer models were generated using spires and roughness elements. Five spires with a height of 1.3 m were placed at the centre-line distance of 0.5 m in the lateral direction. The spires were followed by a 7.2 m fetch of wooden roughness elements of 90 mm × 90 mm cross section and 45 mm height. The roughness elements covered approximately 24% of the floor area over the fetch length. The heliostat model was placed 8.8 m downstream of the spires, which was determined to be sufficient for flow development through measurement of velocity at several streamwise locations. Figure 1 shows a schematic of the setup in the wind tunnel.

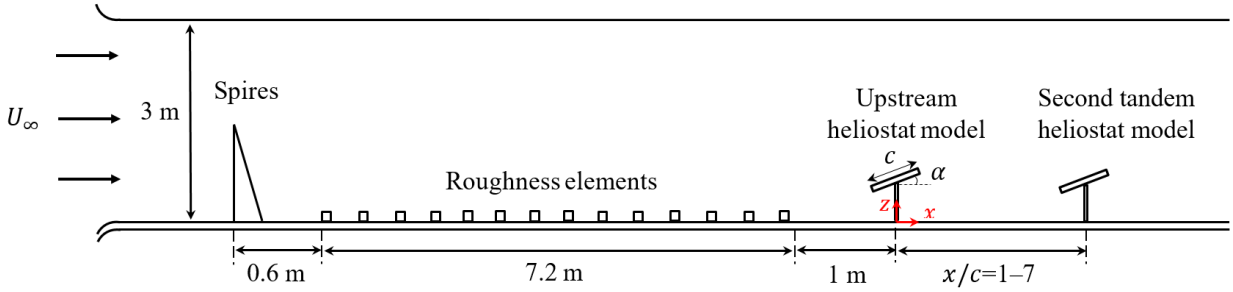

FIGURE 1. Schematic of the experimental setup at the university of Adelaide wind tunnel showing spires and roughness elements and the heliostat models. The gap between the two heliostat models, *x/c*, varies between 1 and 7 in the experiments.

A Turbulent Flow Instrumentation (TFI) multi-hole pressure probe was used to measure the three components of velocity (in *x, y, z* directions) at a sampling frequency of 1kHz, and the mean and turbulence characteristics of the simulated boundary layer were determined from the measured velocity. Figure 2(a–c) show the vertical profiles of mean velocity, turbulence intensity and integral length scales at the position of the upstream heliostat and in the absence of the heliostat models. The thickness of the generated boundary layer is determined to be 1 m, and the mean velocity in the boundary layer is found to match a logarithmic profile with an aerodynamic surface roughness value of 0.002 m. The longitudinal and vertical turbulence intensity at the heliostat hinge height, *H*, shown by the horizontal dashed lines, are approximately 9% and 6%, respectively. For the purpose of this study, similarity of mean velocity and turbulence intensity were only considered. A detailed discussion of the similarities and differences of the turbulence spectra and integral length scales in the wind tunnel and atmospheric boundary layer, and the effect of scaling of turbulence in the wind tunnel is provided in Jafari *et al.* [10].

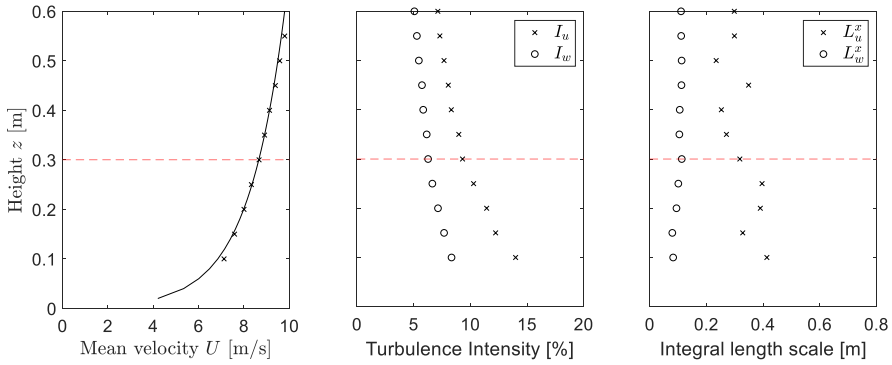

FIGURE 2. Mean velocity and turbulence characteristics in the simulated boundary layer: (a) Mean velocity in the boundary layer compared to the logarithmic profile (the solid line), (b) longitudinal I_u and vertical I_w turbulence intensities, (c) longitudinal L_u^x and vertical L_w^x integral length scales. The horizontal dashed line shows the heliostat hinge height, H.

Two heliostat models were placed in the wind tunnel in tandem arrangement at different elevation angles, α, of 30°, 60° and 90°. In all configurations, both heliostats were elevated at the same angle. Furthermore, the gap between the heliostats was varied between 1 to 7 times the chord length of the mirror panel, c, by moving the second heliostat downstream while keeping the upstream heliostat at a constant position. Figure 3 (a–b) show the heliostat model. The heliostat models were made of a square panel with a chord length of c=0.4 m mounted on a pylon of 0.3 m height. A hinge joint was used, which allows setting the elevation angle of the panel between 0° and 90°. One of the models was equipped with pressure transducers inside the heliostat panel cavity (with a thickness of 22 mm) to measure the differential pressure between the taps on the upper and lower surfaces of the panel, as shown in Fig. 3(c). 30 pressure taps were used on each the upper and lower surfaces of the heliostat panel. *Honeywell TruStability* board- mount pressure sensors with a differential measurement range of ±250 Pa were used. Two *National Instruments* NI-9220 data acquisition modules and the LabVIEW control software were used to collect and convert the measured voltages to the pressure values. The pressure measurements on the second tandem heliostat were conducted for a duration of 180 s at each location at a sampling rate of 1 kHz. The pressure on the upstream heliostat in the absence of the second tandem heliostat, herefater refered to as the single heliostat,was also measured for comparison with the tandem configuration.

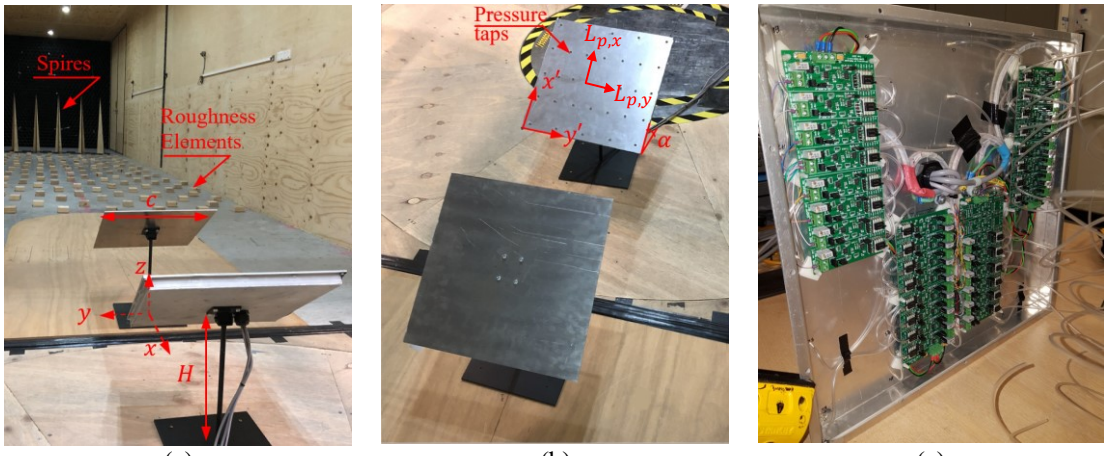

FIGURE 3. (a) The heliostat models and the boundary layer generation setup at the University of Adelaide wind tunnel, (b) the coordinate axes (x',y') for surface pressure measurements, (c) the custom-made pressure transducer boards inside the panel cavity.

The pressure coefficients were calculated from:

$$C_{P_i} = \frac{P_i^f - P_i^b}{1/2\rho U_H^2} \quad (1)$$

where the numerator shows the instantaneous differential pressure between the upper and lower surfaces of the panel at each location. ρ is the air density, and U_H is the mean velocity at the heliostat elevation axis height. In order to compare the pressure coefficients for different tandem configurations, U_H, the mean velocity measured at the location of the upstream heliostat in Fig. 3, is used for all single and tandem cases.

RESULTS AND DISCUSSION

Unsteady Surface Pressure Distributions

Figure 4 shows the time-averaged distributions of pressure coefficient on the second tandem heliostat in comparison with the single heliostat. The mean surface pressure distributions for the single heliostat configurations show a similar pattern to those presented by Gong *et al.* [11], which demonstrates the validity of the currrent measurements. The pressure coefficients are maximum in the centre of the panel for α=90°. As the elevation angle decreases to α=60° and α=30°, the location of maximum pressure coefficients moves closer to the leading edge of the panel.

The mean pressure coefficients of the second heliostat are in general smaller than the single heliostat for *x/c* between 1 and 3 as the second tandem heliostat is shielded by the upstream heliostat. The mean velocity in the wake of the upstream heliostat is lower than the mean velocity in the boundary layer, and thereby the second tandem heliostat is exposed to a lower mean velocity. This blockage effect is more significant for α=90° where the mean pressure coefficients on the tandem heliostat are about one third of those on the single heliostat. At *x/c*= 1, when the tandem heliostat is placed in the near wake of the upstream heliostat, negative pressure coefficients are observed indicating larger pressure at the back of the heliostat panel. The region of negative pressure is mainly concentrated near the leading edge at α=30°, whereas at α=90°, almost the entire panel is exposed to negative pressure. The observed phenomena can be related to the existence of an extended-body flow regime in which the free shear layers from the upstream heliostat overshoot the tandem heliostat resulting in a very low pressure region between the two heliostats. The extended-body flow regime was also observed by Auteri *et al.* [12] to occur for gap ratios up to 1 for two tandem plates at α=90° exposed to a uniform flow and Reynolds numbers of up to 78500.

Regions of high-magnitude pressure similar to the single-heliostat reappear at *x/c*=4. As the gap ratio increases to *x/c* between 5 and 7, and the wake starts to recover, the distribution of the mean pressure coefficients on the heliostat panel becomes similar to that on the single heliostat. The magnitude of the pressure coefficients however remains slightly less than the single heliostat as the tandem heliostat is still exposed to lower mean velocity in the recovering wake flow. The results in Figure 4 show that the time-averaged distribution of pressure on the tandem heliostat does not differ significantly from the distribution on a single heliostat when the gap ratio between the two heliostats is 4 and above.

Figure 5 compares the distribution of peak pressure coefficients on the second tandem heliostat at different gap ratios with the single heliostat. The peak pressure coefficients are calculated as the sum of the mean pressure coefficients and 3-times the standard deviation [13]. The distributions of peak pressure for the single heliostat show a similar pattern to those found by Gong *et al.* [11], in which a region of high-magnitude pressure exists at the leading edge for α=30°, and in the centre for α=90°.

The distribution of peak pressure on the second tandem heliostat at smaller gap ratios differs noticeably from the distribution on a single heliostat, while similar to the trends observed for the mean pressure distribution, the distribution of the peak pressure coefficients are a closer match to the single configuration at larger gap ratios (*x/c*=6–7). For the tandem heliostat at smaller gap ratios (*x/c*=1–4), the largest peak pressure coefficients are found near the edges of the heliostat panel. These high-magnitude regions are exposed to the shear layers separating from the edges of the upstream heliostat imposing a large-magnitude unsteady pressure on them. The high-magnitude peak pressure coefficients are mainly concentrated at the leading edges of the panel at elevation angles of 30° and 60°. The largest magnitude of the peak pressure coefficient at the high magnitude regions occurs at *x/c*=3 for all elevation angles of the heliostat panel. This determines *x/c*=3 as a critical gap ratio for the design of heliostats in the second row of a field exposed to the oncoming wind direction.

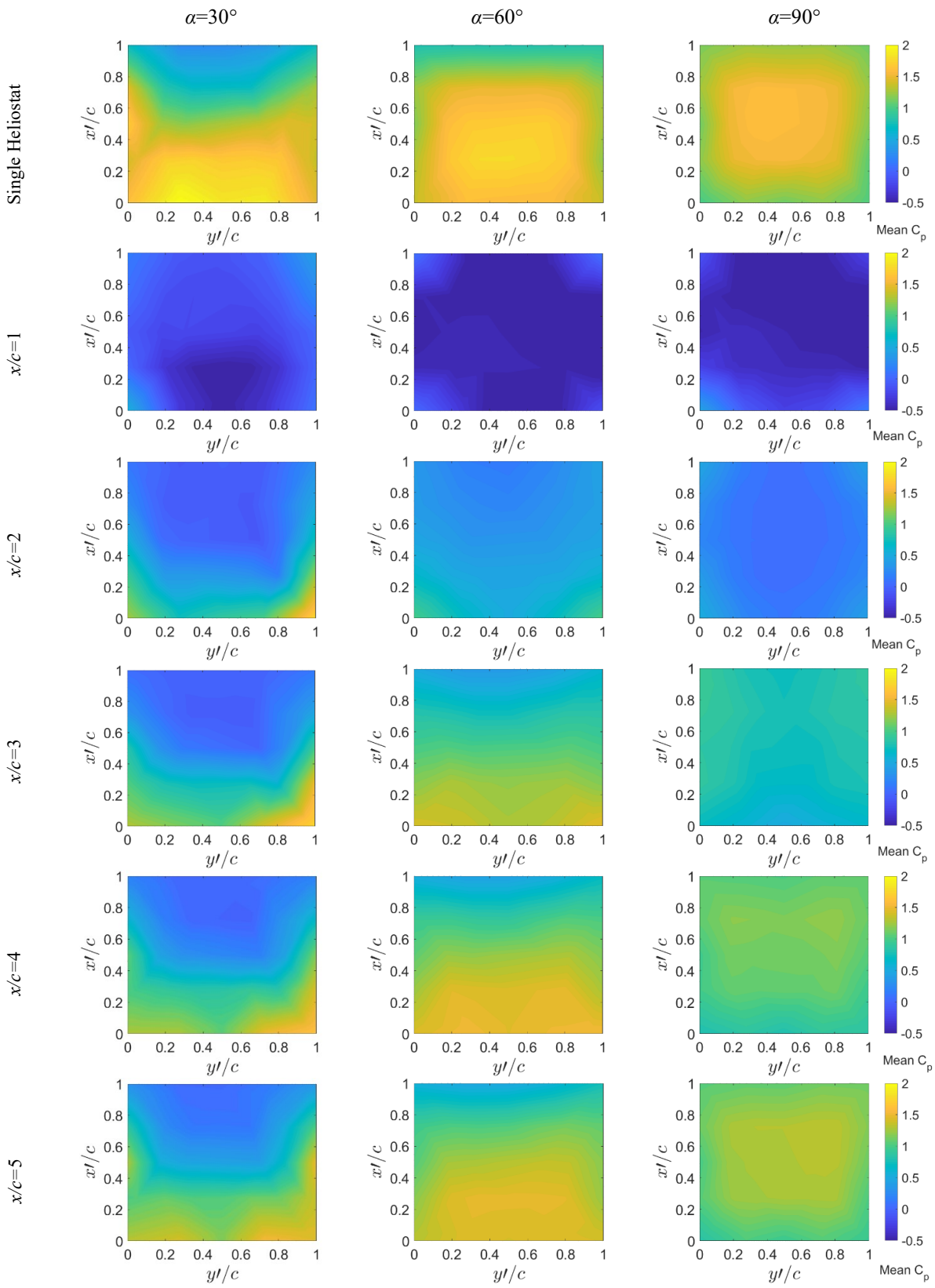
α=30°
α=60°
α=90°
Single Heliostat
x/c=1
x/c=2
x/c=3
x/c=4
x/c=5
x′/c
y′/c
Mean C_p

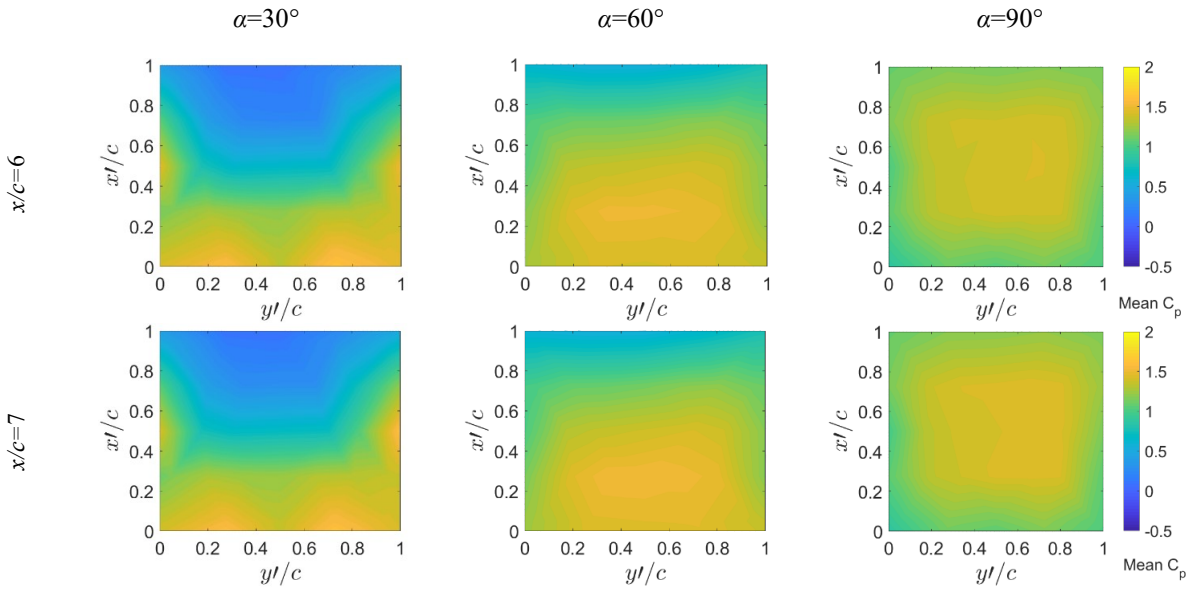

FIGURE 4. Contours of surface distribution of the mean pressure coefficients on the heliostat panel for a single heliostat and the second tandem heliostat at gap ratios, *x/c*=1–7, and different elevation angles α=30°, 60°, 90°.

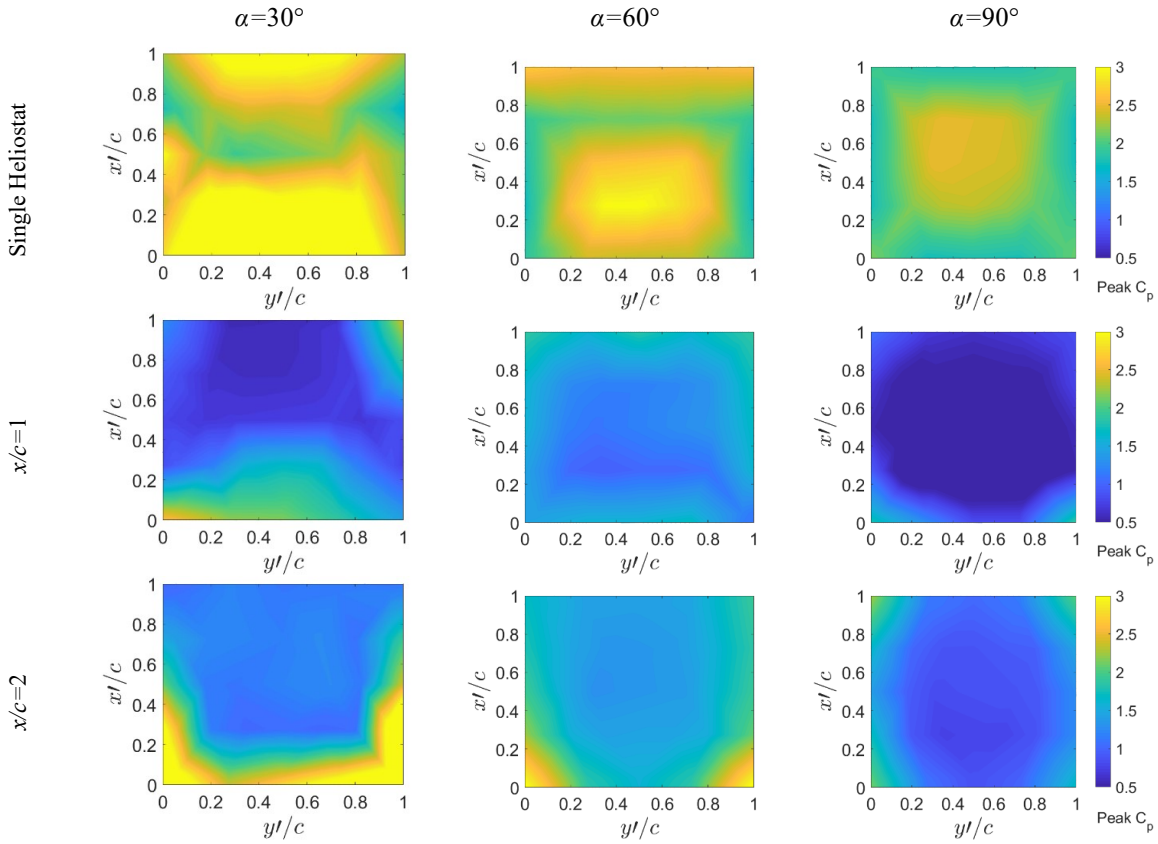

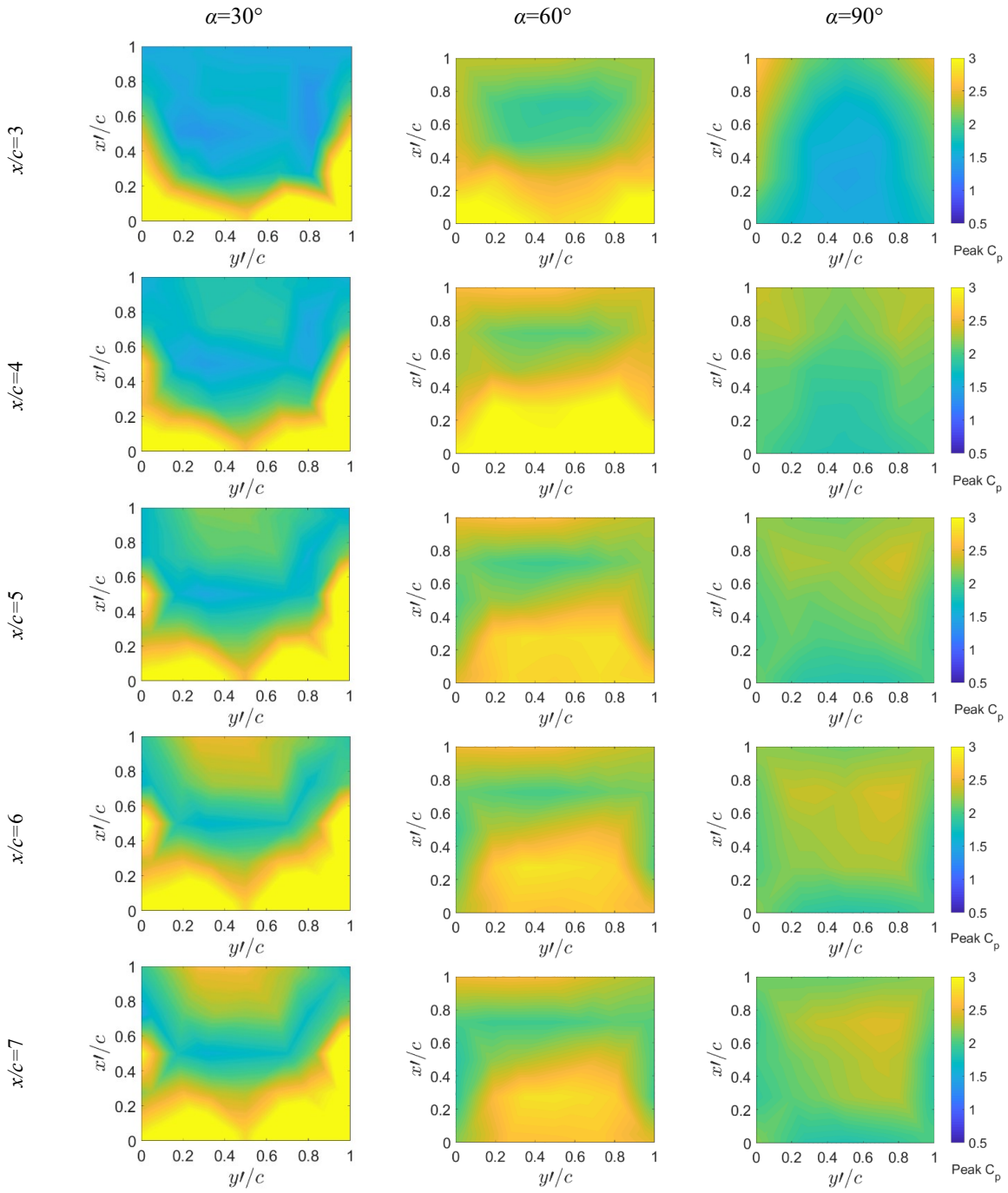

FIGURE 5. Contours of surface distribution of the peak pressure coefficients on the heliostat panel for a single heliostat and the second tandem heliostat at gap ratios, x/c=1–7, and different elevation angles α=30°, 60°, 90°.

Centre of Pressure on the Heliostat Panel

As shown in the mean and peak pressure distributions in Fig. 4 and Fig. 5, the non-uniform pressure distribution on the heliostat panel varies when the gap ratio between the two tandem heliostats changes. The centre of pressure represents the position where the net normal pressure force acts on the heliostat panel. The distance of the centre of pressure from the centre of the heliostat panel ($x'=\frac{c}{2}$, $y'=\frac{c}{2}$) is found from the following [14]:

$$L_{px}=\frac{\int_0^c x'p(x',y')\,dx'}{\int_0^c p(x',y')\,dx'}-\frac{c}{2} \tag{2}$$

$$L_{py}=\frac{\int_0^c y'p(x',y')\,dy'}{\int_0^c p(x',y')\,dy'}-\frac{c}{2} \tag{3}$$

The calculated centre of pressure of the second tandem heliostat for different heliostat gap ratios and elevation angles are displayed in Fig. 6. The centre of pressure of the single heliostat is also shown at x/c=0. The points in the figure show the time-averaged position of the centre of pressure and the error bars represent the standard deviation of the centre of pressure for each configuration. Figure 6(a) displays L_{px}/c for different gap ratios between the tandem heliostats. It is found that the changes in the position of the centre of pressure from the single heliostat configuration are more significant for α=30°, in which L_{px}/c varies from −0.06 for the single heliostat to approximately −0.22 for the second tandem heliostat at gap ratios between 2 and 3. At α=60°, L_{px}/c varies between −0.03 and −0.1 for the range of investigated gap ratios, while the mean L_{px}/c remains near zero for α=90°. As the gap ratio between the tandem heliostats increases, the centre of pressure moves closer to its position for the single heliostat which is consistent with the trend observed for pressure distributions in Fig. 4. The increased distance between the centre of pressure and the centre of the heliostat panel is likely to impose larger hinge and base over-turning moments on the heliostat. Moreover, the standard deviation of the centre of pressure, which represents the fluctuations of the centre of pressure, is much larger at smaller gap ratios, i.e. x/c<5, indicating the significant effect of turbulence in the near wake of the upstream heliostat. Furthermore, the standard deviation of the centre of pressure decreases with an increase of the gap ratio.

Figure 6(b) shows L_{py}/c for different gap ratios between the tandem heliostats. The changes in the mean L_{py}/c are less than 0.05, being largest at α=30°, and it generally remains near zero. The standard deviation of L_{py} is however noticeable at smaller gap ratios with a magnitude of 0.06 at x/c=2. Hence, it can be concluded from the results in Fig. 6(a) and Fig. 6(b) that the unsteady variation of the centre of pressure is a dominant effect at x/c<5. Furthermore, the results show that at α=30° the wake of the upstream heliostat does not recover over the measured gap ratios as both L_{px} and L_{py} differ from their values for the single heliostat even at x/c=7.

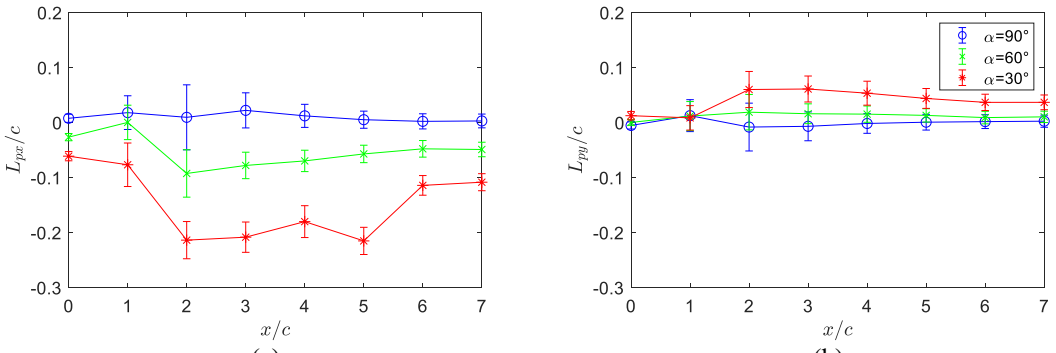

FIGURE 6. Time-averaged position of the centre of pressure for different gap ratios, x/c=0–7, where x/c=0 represents the single heliostat configuration; (a) L_{px}/c, the centre of pressure in x' direction, and (b) L_{py}/c, the centre of pressure in y' direction, measured from the centre of the heliostat panel ($x'=\frac{c}{2}$ and $y'=\frac{c}{2}$) as defined in Fig. 3(b). The error bars show the standard deviation of the centre of pressure from the mean values.

Unsteady Hinge Moment Coefficient

The unsteady variations of the pressure distribution on the tandem heliostat impose unsteady moments at the heliostat hinge and foundation which affect the design of heliostat components. Hence, in this section, the hinge moment, which is critical for the design of the elevation drive, is calculated for the different cases. The unsteady hinge moment coefficient is found as $C_{MHy}=C_{F_N}(L_{px}/c)$, where $C_{F_N}=\oint C_{P_i}\,dA$ is the area-average of pressure coefficients [14]. The mean and peak of the hinge moment coefficient are then determined from the unsteady coefficients. Figure 7(a–b) show the time-averaged and peak hinge moment coefficients on the tandem heliostats and the single heliostat (x/c=0). According to Fig. 7(a), when $x/c\geq3$, the mean hinge moment coefficient is larger than that of the single heliostat for α=30° and α=60°. The larger hinge moment coefficient is due to the increased distance between the centre of pressure and the panel centre (Fig. 6(a)). On the other hand, at $x/c=1$, due to the very small pressure force, the mean hinge moment coefficient on the tandem heliostat is near zero.

The peak hinge moment coefficients show a significant increase at gap ratios equal to and larger than 3 for all elevation angles (Fig. 7(b)) during operation of a heliostat field. This indicates the significant effect of the pressure fluctuations, in terms of both magnitude and distribution, on the tandem heliostat. According to Fig. 7(b), the peak hinge moment coefficient is approximately 40% and 70% larger than the single heliostat at x/c=4 for α=30° and α=60°, respectively. Furthermore, at α=90°, despite the near zero mean hinge moment coefficient, the peak hinge moment coefficient varies between 0.16 and 0.1 for x/c=3 to 7. Furthermore, similar to the mean hinge moment, there is a decrease in the peak hinge moment coefficient at x/c=1 compared to the single heliostat such that the peak hinge moment coefficient at α=30° is 60% less than the single heliostat. Hence, the results show that the unsteady moment at the hinge induced by the surface pressure fluctuations varies significantly depending on the gap between the two heliostats. Therefore, heliostats must be designed according to the variations of wind loads in high-density and low-density areas of a field.

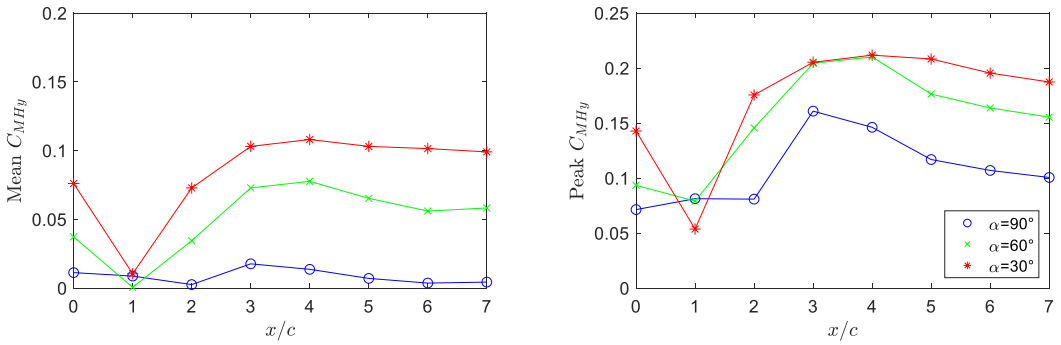

FIGURE 7. (a) The time-averaged, and (b) the peak hinge moment coefficients for α=30°, 60° and 90°, and for different gap ratios, x/c=0–7, where x/c=0 represents the single heliostat configuration.

CONCLUSIONS

The unsteady surface pressure distribution on heliostats in tandem arrangement was investigated in this study. The differential pressure between the upper and lower surfaces of the heliostat panel was measured through wind tunnel experiments for different gap ratios between the tandem heliostats and at different elevation angles of operating heliostats. The results were compared to the surface pressure distributions on a single heliostat. It was found that while the mean pressure coefficients on the second tandem heliostat are in general smaller than the single heliostat for gap ratios between 1 and 3, concentrated regions of large-magnitude peak pressure exist near the edges of the panel. The magnitude of the peak pressure coefficient at the panel edges of the tandem heliostat was the largest at a gap equal to 3-times the panel chord length for all of the investigated elevation angles. The time-averaged position of the centre of pressure was found to differ significantly from the single heliostat at elevation angles of 30° and 60°. Moreover, the results showed that the position of the centre of pressure fluctuates noticeably about its time-averaged position at smaller gap ratios. Hence, in dense areas of a heliostat field, the unsteady variations of the pressure on the heliostats

have a dominant effect on the maximum hinge moments, which must be considered for the design of the heliostat elevation drive. Furthermore, the results indicate that the changes in the unsteady pressure distribution on a heliostat in tandem arrangement significantly affect the peak and unsteady wind loads, such that at $x/c \geq 3$, the peak hinge moment coefficient on a tandem heliostat can increase by 40% and 70% from that of the single heliostat at $\alpha=30°$ and $\alpha=60°$, respectively. Hence, design of heliostats in a field arrangement requires understanding the unsteady wind loads within the field which dependent on the field arrangement can differ significantly from a single heliostat. Moreover, the results suggest the possibility to reduce the cost of heliostats by optimization of the layout of the heliostat field with respect to the wind loads. It is recommended to develop the arrangement of heliostats in a field according to the site terrain type such that the unsteady wind loads on the in-field heliostats will be reduced and therefore by reduction of design wind loads cheaper heliostats can be produced.

ACKNOWLEDGMENTS

Financial support for the project has been provided by the Australian Government Research Training Program, the University of Adelaide Scholarship and the Australian Solar Thermal Research Initiative (ASTRI). The authors would like to acknowledge the School of Mechanical Engineering and the workshops at the University of Adelaide.

REFERENCES

1. J. A. Peterka, Z. Tan, J. E. Cermak and B. Bienkiewicz, Journal of Solar Energy Engineering **111**, 158-164 (1989).
2. A. Pfahl, Eindhoven: Technische Universiteit Eindhoven (2018).
3. M. J. Emes, M. Arjomandi, F. Ghanadi and R. M. Kelso, Solar Energy **157**, 284-297 (2017).
4. A. Jafari, F. Ghanadi, M. Arjomandi, M. J. Emes and B. S. Cazzolato, Journal of Wind Engineering and Industrial Aerodynamics **189**, 218-230 (2019).
5. T. M. Hui, Master of Engineering, Universiti Tunku Abdul Rahman (2011).
6. J. A. Peterka, N. Hosoya, B. Bienkiewicz and J. E. Cermak, Technical Report for Colorado State University (1986).
7. J. A. Peterka, L. Tan, B. Bienkiewcz and J. E. Cermak, Technical Report for Colorado State University (1987).
8. M. J. Emes, F. Ghanadi, M. Arjomandi and R. M. Kelso, Renewable Energy **121**, 548-558 (2018).
9. J. S. Yu, M. J. Emes, F. Ghanadi, M. Arjomandi and R. Kelso, Solar Energy **183**, 248-259 (2019).
10. A. Jafari, F. Ghanadi, M. J. Emes, M. Arjomandi and B. S. Cazzolato, Journal of Wind Engineering and Industrial Aerodynamics **193**, 103955 (2019).
11. B. Gong, Z. Wang, Z. Li, C. Zang and Z. Wu, Renewable Energy **50**, 307-316 (2013).
12. F. Auteri, M. Belan, C. Cassinelli and G. Gibertini, Journal of Visualization **12** (4), 307-321 (2009).
13. E. Simiu and R. H. Scanlan, *Wind Effects on Structures*. (John Wiley & Sons, 1996).
14. M. J. Emes, A. Jafari, F. Ghanadi and M. Arjomandi, AIP Conference Proceedings **2126** (1), 030020 (2019).